Modeling Nonpenetrating Ballistic Impact on a Human Torso

Jack C. Roberts, Paul J. Biermann, James V. O'Connor, Emily E. Ward, Russell P. Cain, Bliss G. Carkhuff, and Andrew C. Merkle

When soldiers or law enforcement officers are shot in the chest or abdomen there may be internal injuries even though a soft armor vest prevents penetration of the projectile. This nonpenetrating injury could remain undetected until the person succumbs, for instance, to hemorrhaging in the lungs or laceration of the liver. In addition, tools are needed to design more effective soft armor vests that are lightweight, are flexible enough to fit the body contour, and can defeat high-velocity rifle rounds. To study internal organ injuries and design better vests under nonpenetrating ballistic impact, both a computational (finite element) model (FEM) and a physical human surrogate torso model (HSTM) have been developed. These models consist of the heart, lungs, liver, and stomach surrounded by the skeleton. The HSTM was outfitted with a soft armor vest, and ballistic tests were conducted using 9-mm ammunition at various velocities. While the peak accelerations and peak pressures from the FEM did not match those from testing, the trends and patterns were similar. These results represent a significant step in developing an understanding of the deformations and energy transfer characteristics of ballistic impacts through personal body armor.

INTRODUCTION

To better understand the injury mechanisms of nonpenetrating high-speed (ballistic) impact and assist in the design of personal protective armor for soldiers or law enforcement officers, a program was undertaken to develop both a computational (finite element) and an experimental model of the human torso. The following literature survey of these models is included here to orient the layperson in the subject.

Computational Models

One of the first finite element models (FEMs) of the thorax used linear elastic material properties (neglecting soft tissue properties) and only imposed static loads on the sternum.[1] In subsequent studies, this same model was used for a dynamic modal synthesis technique.[2,3] Each visceral subsystem was represented by either a mass-spring-damper discrete model or a three-dimensional (3-D) solid element model, depending on the

required detail in the viscera. Only the skeletal stiffness was simulated (the visceral stiffness was discounted), and the mass was lumped at discrete nodal points around the chest wall.

Later, a two-level "thorax/subsystem" modal synthesis method was used to expand the baseline model.[4] This model is similar to the previous one but has the capability of incorporating the visceral subsystem. In another study, two half-symmetry models were formulated to save computing time.[5] The first model consisted of a skeletal cage containing elements representing a portion of the vertebral column, the sacrum, the coccyx, ribs 1 through 10, and the sternum. The second model was that of the full thoracic body, including muscle and gross internal organs. Linear elastic behavior was assumed for all materials.

More recently a 3-D model of the thorax was created for frontal impact simulation.[6] This, as well as an earlier model,[7] contained a much better physical description of the human thorax than previous models. Although the ribs, sternum, spine, muscles, and some cartilaginous ligaments were modeled, the separate internal organs were not. Linear elastic material properties were assumed for all elements except for the interior elements, where a viscoelastic model was used.

Another more recent model includes the complete musculoskeletal structure (ribs, sternum, vertebrae, discs, cartilage, and muscle) as well as internal organs (heart, lungs, thoracic aorta, esophagus, trachea, diaphragm, and mediastinum).[8] Viscoelastic properties were used for the organs and elastic properties for bone.

The latest model found in the literature included not only the ribs, sternum, and vertebral column but muscle as well[9] and employed elastic properties for bone and viscoelastic properties for the muscle. However, even the latest models use incorrect elements, particularly for the ribs, and generally lack an adequate number of elements to describe the strains and stresses imposed under ballistic impact.

Experimental Models

In addition to postmortem human subjects and animal subjects (pig, sheep, etc.), there are a number of other test devices for studying ballistic impact. The Naval Research Laboratory has developed a torso consisting of silicone named "Gelman." This model can be used with a soft armor vest to run ballistic tests or in blast tests to identify the pressures and shock waves generated through the gel. Hybrid III anthropometric test devices (ATDs; "crash test dummies"), originally designed to duplicate the kinematic motion of a human in automotive crash testing, have also been used in ballistic testing. ATDs consist of steel and aluminum parts for the bones (rib cage, vertebral column, femur, tibia, etc.), covered by a thick layer of a tough polymer to represent muscle, fat, and skin. This makes for a very rugged surrogate. The ATDs have accelerometers and load transducers located throughout.

Another anthropometric dummy consisted of wood, water, and plastic[10,11] and was designed specifically for blast, blunt impact, and missile testing. The lungs were constructed of two pieces of cylindrical plastic foam with a total volume approximately equal to that of an adult and were positioned within a water-filled torso. The head was made of wood with airways and pressure transducers corresponding to tympanic membranes. A pressure transducer was also placed in the center of each lung for recording intrathoracic pressures and peak overpressures.

The Australian government has supported the development of a physical human torso model with some internal organs and an aluminum rib cage. However, the authors could find no published information on it.

All of these models suffer from inadequate anthropometry and lack proper soft and hard tissue properties.

ANALYSIS

Recall that the purpose of this investigation was to develop an improved computational model and an experimental model of the human torso to predict injury from nonpenetrating ballistic impact. An FEM of a 5th-percentile male torso was created that included the skeleton (ribs, sternum, cartilage, and vertebral column) along with the heart, liver, lungs, stomach, muscle, and skin. Linear elastic properties were used for bone and viscoelastic properties were used for all internal organs and viscera. A physical human surrogate torso model (HSTM) was developed with the same anthropometry as the FEM and included all the same components. The bones were fabricated to have the tensile properties of human cancellous bone, and the organs were designed to have the correct density and hardness of porcine (pig) organs, which are very similar to human organs. Piezoelectric pressure sensors were placed in the organs, and flexural sensors were attached to the ribs. An accelerometer was mounted to the posterior surface sternum. The HSTM was tested under ballistic impact conditions, and a comparison was made with FEM results.

Methods

Finite Element Model

The surfaces of the upper thorax (rib cage, spine, heart, lungs, liver, and stomach as well as the skin and muscles) were obtained from Digimation (St. Rose, LA) and imported into the finite element code IDEAS. The ribs and vertebral column were divided into ribs, cartilage, sternum, and vertebral column. Figure 1 shows the components of the torso model in an expanded view. In Fig. 1a, the skin and muscles are represented with the global coordinate system display. The coordinate

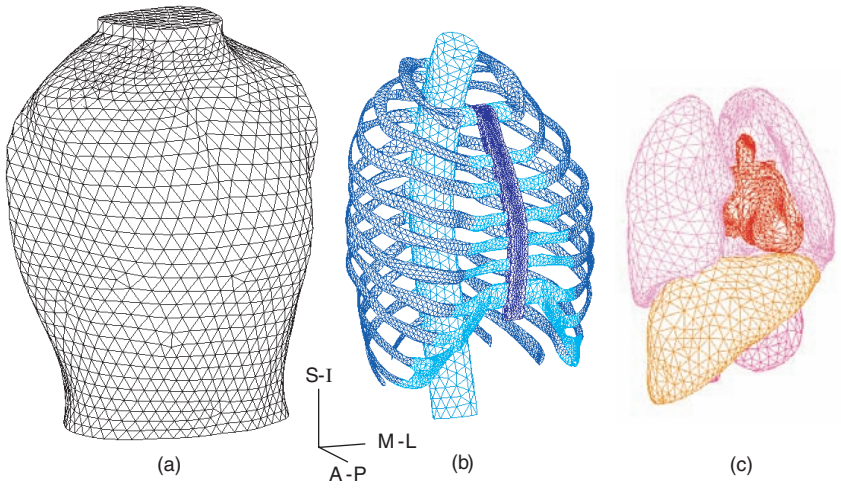

Figure 1. Exploded model view: (a) skin/muscles, (b) skeletal structure, and (c) internal organs.

system is defined as the anterior-posterior (A-P) direction, medial-lateral (M-L) direction, and superior-inferior (S-I) direction represented by the triad *x*, *y*, and *z*, respectively. Figure 1b shows the ribs, cartilage, sternum, and vertebral column, and Fig. 1c shows the heart, lungs, liver, and stomach. Linear solid tetrahedral elements were used for the organs, mediastinum, and diaphragm as well for the skeletal structure (ribs and sternum) and vertebrae.

Figure 2 shows a cutaway of the torso with the skeleton, heart, lungs, liver, stomach, mediastinum, muscle, and skin. Elastic properties for the ribs, sternum, and vertebral column were taken from the literature.[8,12] Since muscle and skin cannot carry compressive loads, they were modeled using membrane shell elements. The static model was then exported to the explicit finite element code LS-DYNA (Liverware Software, Livermore, CA). In the dynamic model, the internal organs do not share nodes; rather, they transfer loads through the definition of contact interfaces between the various components. This provides for slip at the boundaries between all organs and between the organs and the skeletal structure. Therefore, in LS-DYNA the slip condition was enforced by assigning a low dynamic coefficient of friction (0.0003) between the organs.

A viscoelastic material model from LS-DYNA was used to model soft tissue components (heart, lungs, liver, stomach, mediastinum, as well as muscle and skin). This model does not describe the different types of tissue behavior in detail, but provides a first approximation of the gross behavior. The viscoelastic properties for the internal organs were taken from Refs. 6 and 12. These properties were obtained by using the response of cadavers in automotive impact tests in an effort to iterate the constitutive models and eventually obtain the appropriate organ properties. In these models, the properties were subsequently used for internal organs.

National Institute of Justice (NIJ) Type II body armor was then added to the model. The material properties for the armor were determined through internal testing with Kevlar fabric. The elastic modulus of Kevlar fabric in either the warp or fill directions falls into a low-strain, low-stiffness region in which there is progressive uncrimping of the fabric.[13] Young's modulus in the first region is denoted as E1. This is followed by a higher stiffness region in which the yarns are fully tensioned and the Young's modulus increases with E2 > E1. For plain-weave, 850-denier KM2, E1 and E2 were 7.4 and 74.0 GPa, respectively.[14] This presupposes that the fabric, when loaded, will be strained enough to reach the second region; however, that may not be the case. When the fabric is fitted around a person's chest, the boundaries are not constrained and the total layers of fabric can easily move and greatly reduce the strains that would exist if the boundary were fixed. Therefore, the stiffness of the material would appear lower than that at the high-strain rate. As a result, the lower elastic modulus of 7.4 GPa was used for the vests in this analysis.

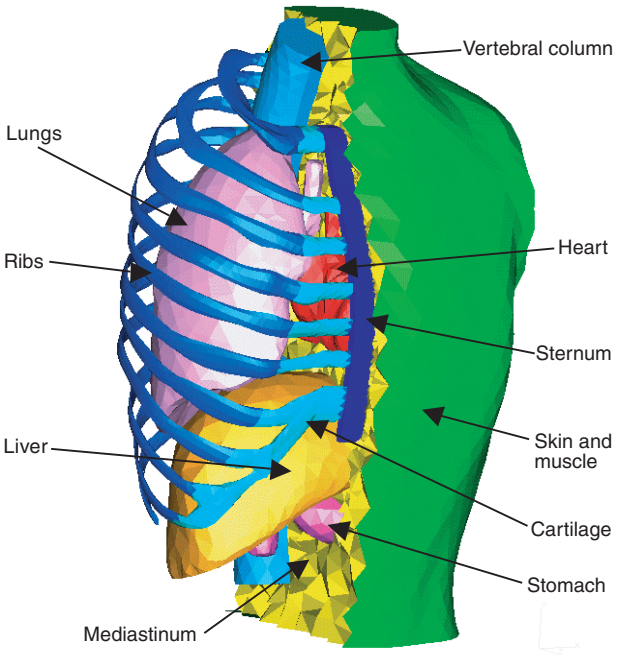

Figure 2. Cutaway view of the model showing all the major components to be assembled.

The 9-mm (8-*g*) projectile was modeled with 60 hexahedral and pentahedral solid elements. The kinematic plastic material model (Material Model 3) was used to model the plastic deformation of the bullet to ensure proper energy transfer to the armor, and subsequently, to the torso.

Physical Human Surrogate Torso Model

All components previously created in LS-DYNA were translated into individual 3-D component files and exported to the Stratasys FDM (Stratasys, Inc., Eden Prairie, MN) rapid prototype station at APL. Figure 3 shows the finished surrogate organs. The specific steps used in fabrication varied by component type.

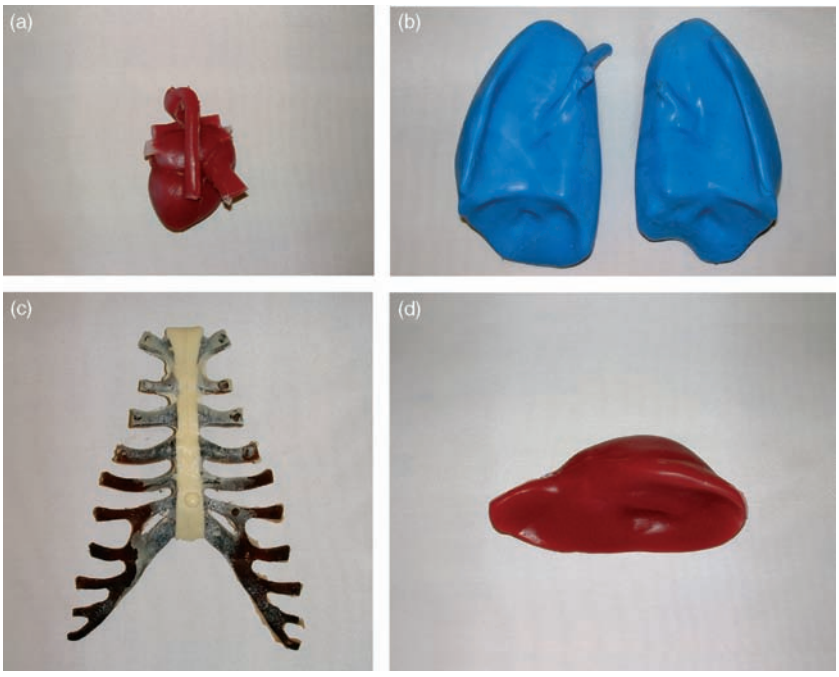

Figure 3. Human organ surrogate components: (a) heart, (b) lungs, (c) sternum and cartilage, and (d) liver.

Once the organs and skeleton were completed, piezoelectric pressure sensors (PCB Piezotronics Electronics Division, Depew, NY) were embedded in the organs and an accelerometer (Endevco Corp., San Juan Capistrano, CA) was attached to the back of the sternum. One piezoelectric sensor was placed in the heart and stomach and two were placed in the lungs and liver as shown in Fig. 4. Figure 5a shows the skeleton with sensors in the organs and Fig. 5b shows the complete HSTM with skin and muscle.

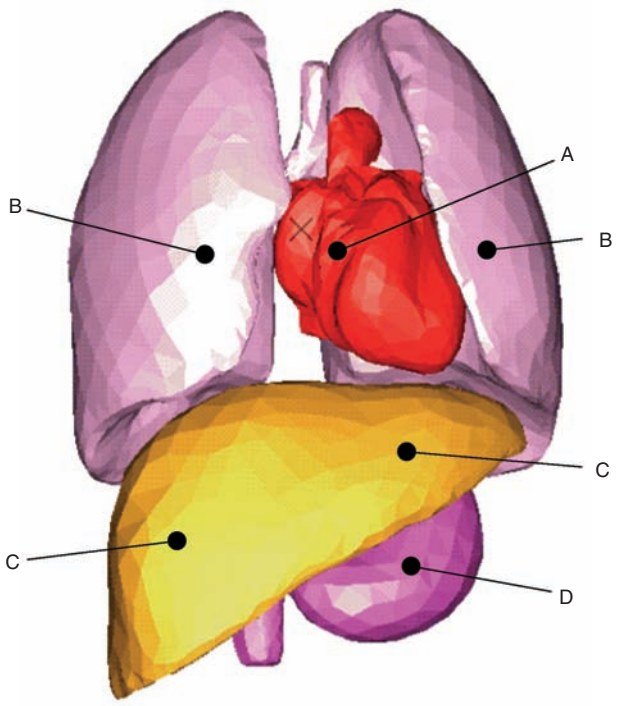

Figure 4. Location of piezoelectric pressure sensors. A: Middle of the heart over the sternum. B: Inside the lung. C: In the right and left halves of the liver. D: Approximately in the middle of the stomach. (Pressure sensor 138M103/003AW: range = 68,950 kPa, sensitivity = 0.013 pC/kPa, rise time <0.5 ms. Charge amplifier 422E12: frequency response = 100 kHz, conversion = 10 mV/1 pC. Signal conditioner 482A22: frequency response = 0.1 to 1 MHz. Accelerometer 7270A-60K: measurement range = 60,000 *g*, frequency response = 100 kHz.)

Testing

The HSTM was taken to the H. P. White ballistics laboratory (Street, MD) for testing. The model was outfitted with an NIJ Level II Kevlar vest, which was positioned over the torso for ballistic tests run with 9-mm (8-*g*) ammunition at different velocities. The vest was moved after each test to prevent two bullets from hitting the same point. A TDAS Pro data acquisition system (Diversified Technical Systems, Seal Beach, CA) with a data collection rate of 75 kHz was used to record data from the accelerometer and piezoelectric pressure sensors. An IMC Phantom 4 digital video camera (Vision Research, Inc., Wayne, NJ) was used to capture the events at a data rate of 3700 frames per second. Figure 6 shows the target locations on the HSTM: middle of the sternum anterior to thoracic vertebra T6; over the right and left lung, 6 cm from the center of the sternum; and over the liver subxiophoid at thoracic vertebra T12 (A, B, and C, respectively).

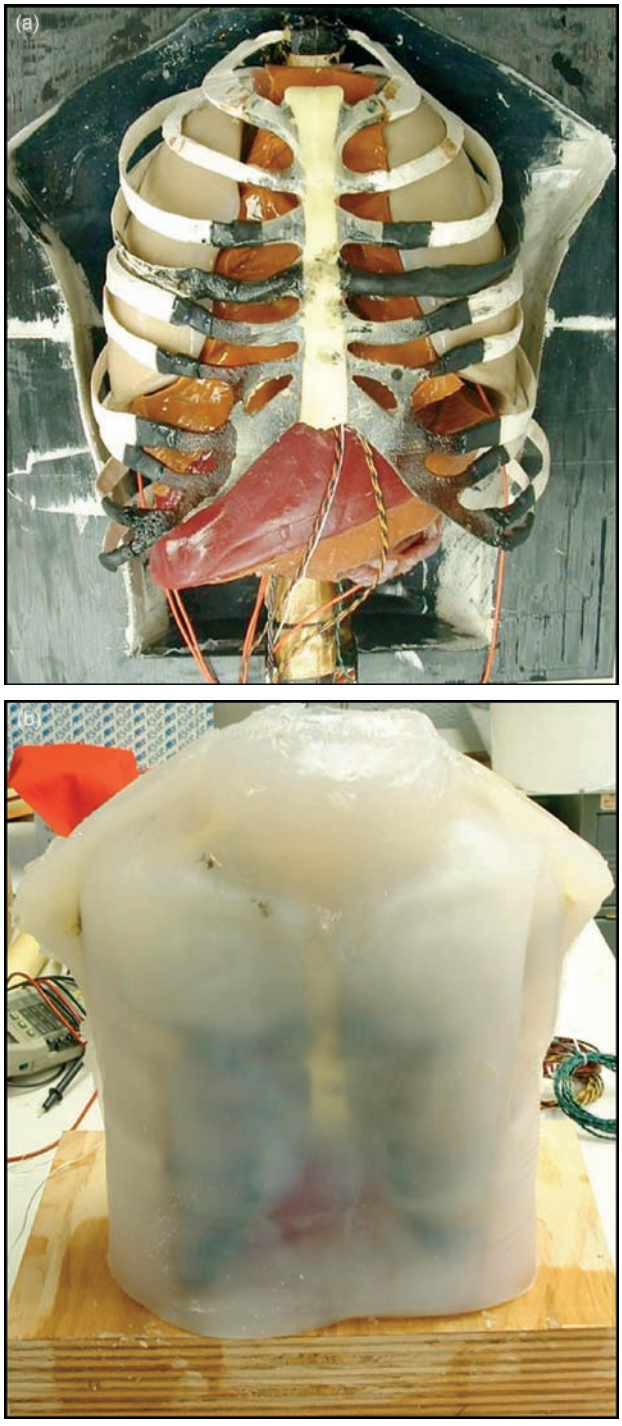

Figure 5. Skeletal structure with all internal organs (a) and final assembled HSTM with skin and muscle (b).

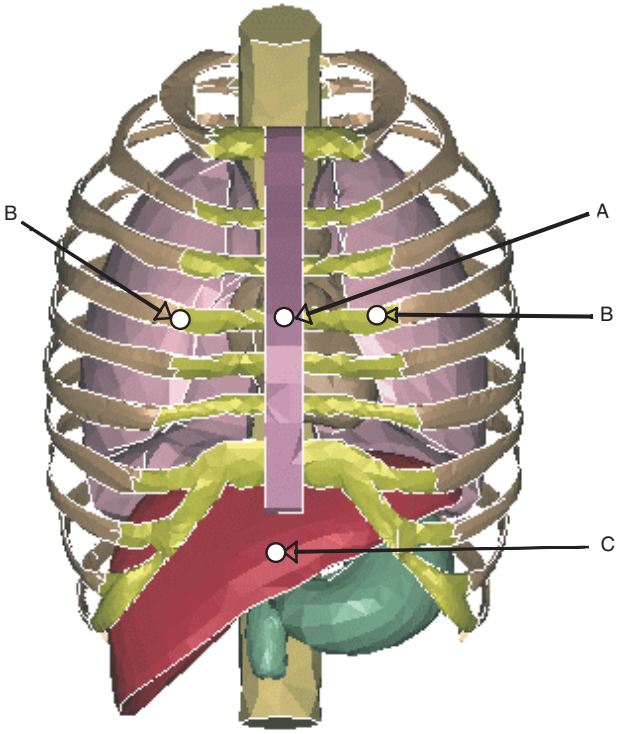

Figure 6. Bullet impact locations. A: At the center of the sternum anterior to T6. B: Over the right and left lung, 6 cm from the midline. C: Over the liver subxiophoid at T12.

Results and Discussion

Figure 7 is a typical plot of sternum acceleration versus time for the experimental test and FEM results from a 9-mm bullet impacting the middle of the sternum anterior to T6 at a velocity of 270 m/s. The absolute magnitude of the peak accelerations from the experimental test are between 4 and 10 times over those of the FEM. Some of the discrepancy could be due to the difference in viscoelastic properties between the synthetic organs and the properties used to describe the material models employed in the FEM. Another contribution to the discrepancy may have been the mechanism used to simulate articulation between the ribs and the vertebral column.

The ribs in the human thorax articulate with one vertebra above and below it. Therefore, to allow some rotation at the rib/vertebrae interface, the ribs in the HSTM were tied and adhesively bonded to the vertebral column with Kevlar fiber bundles. Upon further consideration, it was realized that with the attachment of the ligament at the non-articulating part of the tubercle and with associated musculature, the rib was not free to rotate. This may cause some discrepancy between the FEM, where there is no rotation at the rib/vertebral column interface, and the HSTM, where there is some flexibility at the rib/vertebrae interface.

However, similarities can be seen between the acceleration versus time profiles in Fig. 7. There is an initial negative (inward) sternum acceleration at impact, and the peak occurs at almost the same time for the FEM and the HSTM test results (0.2–0.3 ms) in all cases. For all bullet velocities, the initial negative spike is followed by a positive (outward) acceleration. In the human thorax subject to impact, the energy-absorbing properties of the organs, as with any viscoelastic material, should cause a dampening effect on vibrations

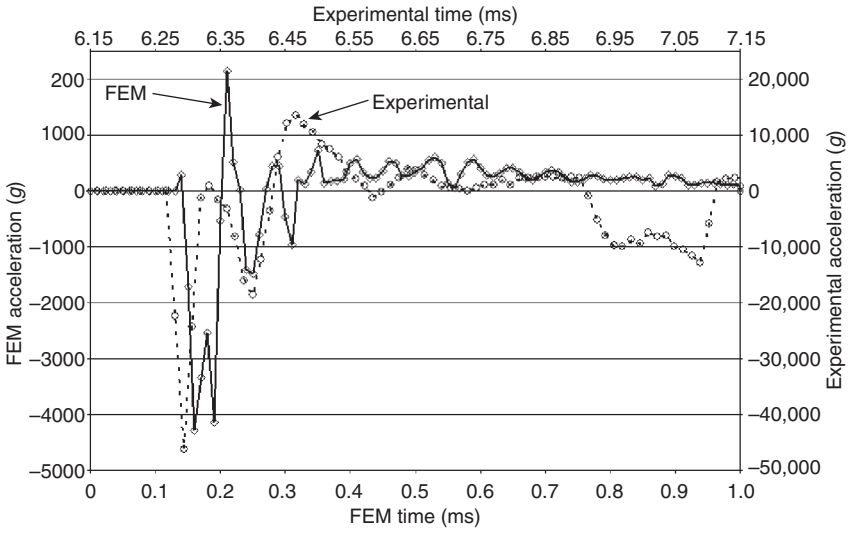

Figure 7. Comparison of experimental and FEM acceleration of the sternum for a 9-mm bullet at 270 m/s impacting on the middle of the sternum anterior to T6.

Figure 9 is a typical FEM and ballistic pressure versus time plot for impact on the middle of the sternum anterior to T6 for 9-mm ammunition impacting at 200 m/s. Notice that the pressure in the heart was higher and occurred sooner than in the other organs in both the FEM and the test results. When impact occurred over the sternum, the magnitude of the pressure in the heart was found to be higher than in the other organs. The pressure in the heart for the FEM and HSTM results increased with an increase in bullet kinetic energy; however, at this time, only qualitative comparisons should be made between the experimental and computational models.

It is evident that although the data traces provide similar trends, the peak pressures and the order in which they occur in the organs are not alike. When comparing impact over the right lung anterior to T6, sternum (heart) anterior to T6, and liver subxiophoid at T12, at the same velocity (200 m/s), the maximum peak pressures in both the FEM and HSTM test results occurred in the organs directly under the impact sites. When the impact site was over felt in the body. This effect was seen in both the ballistic test results (acceleration and pressure data) and the FEM results. It is also evident from the figure that the experimental acceleration of the sternum does not drop off to zero but tends to oscillate and, owing to the damping effect, is attenuated with time. This was also seen when the HSTM was photographed from the side during ballistic impact testing using a 9-mm bullet at a velocity of 360 m/s impacting the middle of the sternum anterior to T6 (Fig. 8).

Another source of error may be the rate of data sampling between the FEM and the HSTM. There was less apparent clipping of the experimental accelerations in the current study compared to that seen in tests with postmortem human subjects.[15] In this study, a 20,000-*g* Endevco 7270A accelerometer with a frequency response of 50 kHz (±5%; 20 μs) was sampled at 100 kHz (10 μs). After examination of the data, it was estimated that the frequency range should be increased to 110 kHz (9.1 μs).

Two test conditions were selected to compare average peak pressures in the organs for a velocity of 200 m/s at two different impact locations (anterior to T6 over the right lung and over the liver subxiophoid at T12).

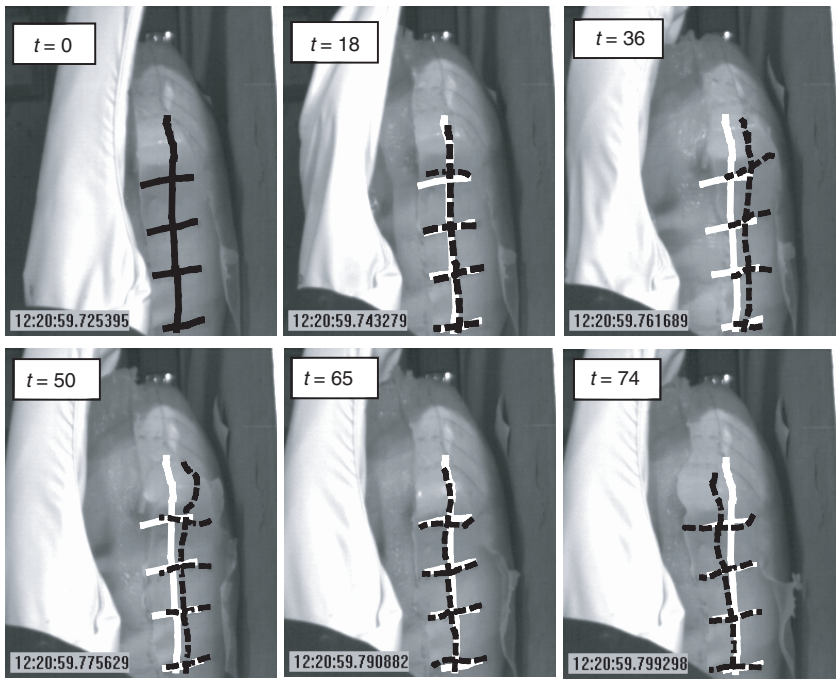

Figure 8. High-speed photographs showing the torso's response to ballistic impact for a 9-mm bullet at 360 m/s. The first image (upper left) displays time zero when impact occurs. The remaining images display sequential times during the impact. The original (white) and deformed (black) torso reference markers are superimposed.

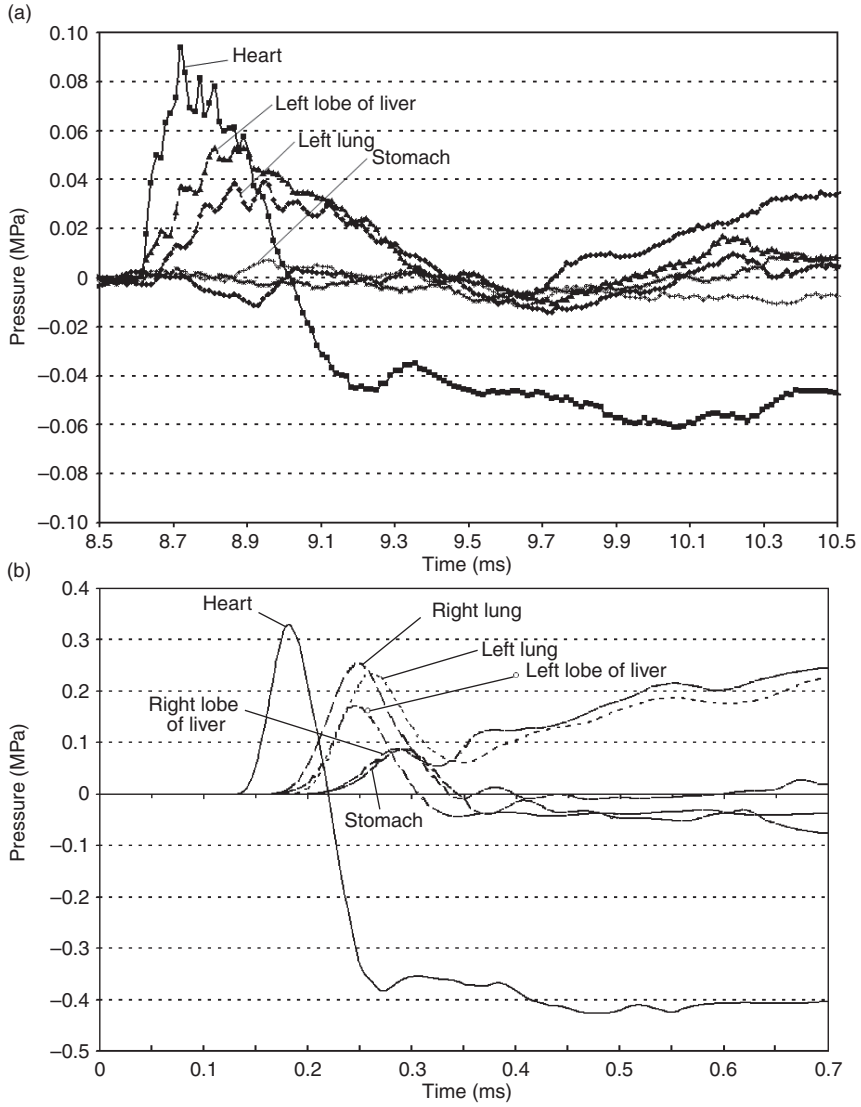

Figure 9. Pressures in the organs for a 9-mm bullet at 200 m/s impacting the Kevlar-protected HSTM in the mid sternum ("A" in Fig. 6): (a) experimental and (b) FEM.

soft tissue (Fig. 10), the typical experimental and FEM pressures in the liver directly beneath the impact point were 2 to 10 times higher, respectively, than the pressures seen in the heart directly under the sternum (Fig. 9). Again, as with the accelerations, these differences were thought to be due to the fixity of ribs to the vertebral column and the differences in viscoelastic properties between the physical model (HSTM) and those used in the FEM. In addition, because of the electrical charging effect of silicone, the piezoelectric sensors are being replaced by higher-frequency piezoresistive sensors, and data acquisition systems with higher sampling rates will also be used to more accurately measure the pressures.

CONCLUSIONS

This work represents several advances, as investigations in the past (to the best of the authors' knowledge) have been done without benefit of physical models of the human torso to adequately describe the pressures and deformations of a torso under ballistic impact, models that measure the pressures in soft tissue (organs), and models of a human torso that can be used to design soft armor.

Both computational and experimental models of the human torso were constructed to model ballistic impact. The upper torso of a 5th-percentile male was modeled to include the ribs, sternum, cartilage, vertebral column, heart, lungs, liver, stomach, muscle, and skin. Viscoelastic properties were used for the organs and linear elastic properties for the skeleton. Organs in the experimental HSTM were designed to have the durometer hardness and density of human or pig organs. Simulated bones in the skeleton were formulated to have the same elastic modulus and Poisson's ratio as those of animal bone.

The FEM was exercised using the equivalent mass and shape of a 9-mm bullet shot at velocities of 150, 200, 270, and 360 m/s. Comparison in the acceleration data between the FEM and experimental HSTM results indicated that the acceleration versus time profiles were similar and increased with increasing kinetic energy, but the magnitudes did not match. The pressures within the organs in both the FEM and HSTM results indicated qualitative agreement, but the peak pressures did not. The pressure versus time profiles for the FEM and HSTM results were very similar; magnitude differences could be due to the difference in viscoelastic properties, poor constraints of ribs to vertebral column in the HSTM, a charging effect that was seen in the piezoelectric sensors, and the frequency range of both the sensors and the data acquisition systems.

Results to date are very encouraging in that the enhanced FEM and experimental models developed at APL are a significant improvement in modeling actual behavior. Hence, this work is worth refining to attain the ultimate goals of understanding injury thresholds and designing better soft armor for a person under nonpenetrating ballistic impact.

In the future, the condition of the rib/vertebral column interface in the HSTM will be modified to fit

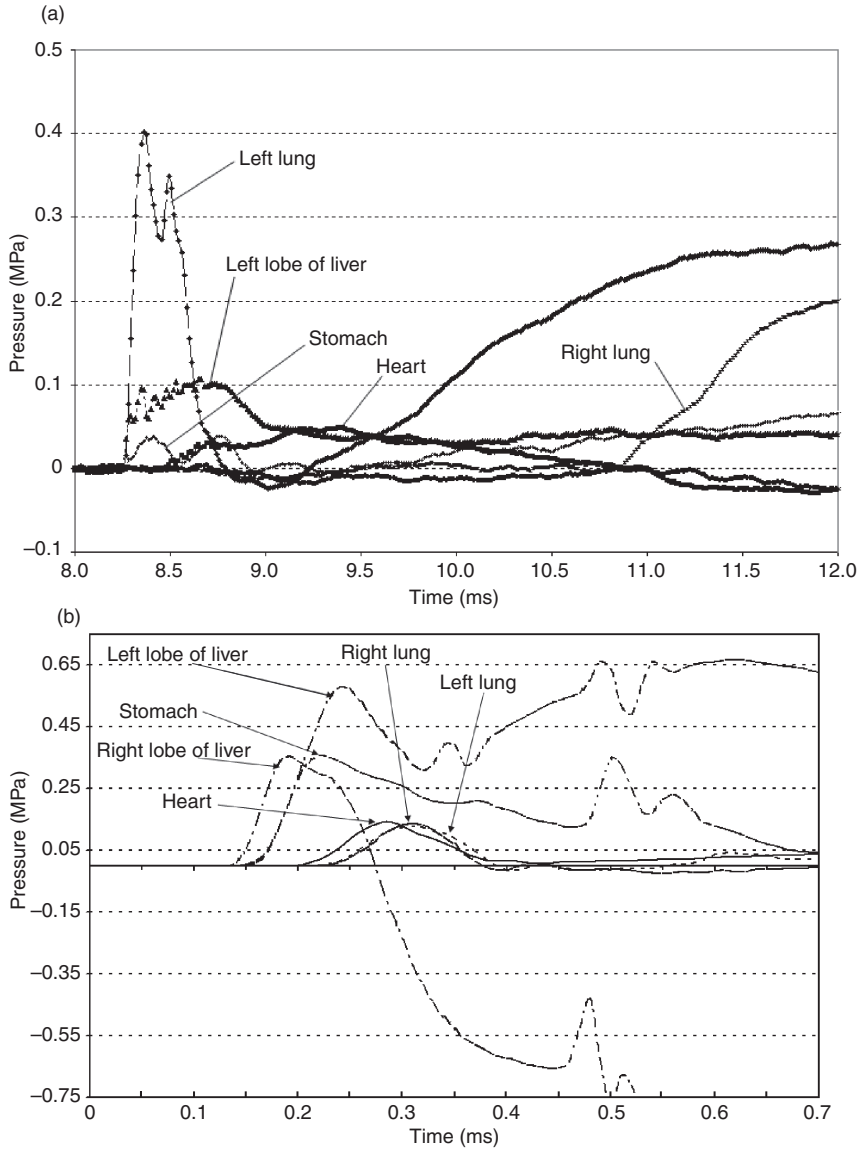

Figure 10. Pressures in the organs for a 9-mm bullet at 200 m/s impacting the Kevlar-protected HSTM directly below the sternum over the liver ("C" in Fig. 6): (a) experimental and (b) FEM.

that of the FEM. The bone composition in the HSTM will be modified to have the fracture properties of human bone, and the proper viscoelastic properties from ongoing split-Hopkinson bar tests will be used for the replacement organs in the HSTM and the FEM. As stated previously, the piezoelectric sensors are being replaced with higher-frequency piezoresistive sensors. The FEM and the HSTM are being modified to include detailed lungs (bronchi), heart (right and left atrium, right and left ventricle, and aortic arch), and intestines to study the effects of thermobaric blast.

Patent No. 6,769,286 has been awarded on the HSTM.

REFERENCES

[1]Roberts, S. B., and Chen, P. H., "Elastostatic Analysis of the Human Thoracic Skeleton," *J. Biomechanics* **3**, 527–545 (1970).

[2]Chen, P. H., *Dynamic Response of the Human Thoracic Skeletal System to Chest Impact*, Ph.D. dissertation, University of California at Los Angeles (1973).

[3]Chen, P. H., and Roberts, S. B., *Dynamic Response of the Human Thoracic Skeleton to Impact*, ENG-0274, School of Engineering and Applied Science, University of California at Los Angeles (1974).

[4]Chen, P. H., "Finite Element Dynamic Structural Model of the Human Thorax for Chest Impact Response and Injury Studies," *Aviat. Space Environ. Med.* **49**(1), 143–149 (Jan 1978).

[5]Sundaram, S. H., and Feng, C. C., "Finite Element Analysis of the Human Thorax," *J. Biomechanics* **10**, 505–516 (1977).

[6]Plank, G. R., Kleinberger, M., and Eppinger, R. H., "Finite Element Modeling and Analysis of a Thorax/Restraint System Interaction," in *Proc. 42nd STAPP Car Crash Conf.*, SAE-P337, pp. 317–329 (1998).

[7]Plank, G. R., and Eppinger, R. H., "An Improved Finite Element Model of the Human Thorax," in *Proc. 13th Enhanced Safety of Vehicles (ESV) Conf.*, pp. 902–907 (1991).

[8]Wang, H. C., *Development of a Side Impact Finite Element Human Thoracic Model*, Ph.D. thesis, Wayne State University, Detroit, MI (1995).

[9]Jolly, J. E., and Young, K. W., *Computer Modeling and Simulation of Bullet Impact to the Human Thorax*, NPS-ME-00-002, Naval Postgraduate School, Monterey, CA (Jun 2000).

[10]Jönsson, A., Clemedson, C. J., and Arevbo, E., "An Anthropometric Dummy for Blast Research," in *Proc. 1983 Int. Conf. on Protective Clothing Systems*, Stockholm, Sweden, pp. 89–97 (Aug 1981).

[11]Jönsson, A., Arvebo, A., and Schantz, B., "Intrathoracic Pressure Variations in an Anthropometric Dummy Exposed to Air Blast, Blunt Impact and Missiles," in *Proc. 5th Symp. on Wound Ballistics* **28**(1), pp. S125–S131 (Jan 1988).

[12]Duck, F. A., *Physical Properties of Tissue*, Academic Press, London (1990).

[13]Grosberg, P., *The Tensile Properties of Woven Fabrics—Structural Mechanics of Fibers, Yarns and Fabrics 1*, J. W. S. Hearle, P. Grosberg, and S. Backer (eds.), Wiley-Interscience, New York, pp. 339–354 (1969).

[14]Johnson, G. R., Beissel, S. R., and Cunniff, P. M., "A Computational Model for Fabrics Subjected to Ballistic Impact," in *Proc. 18th Int. Symp. on Ballistics 2*, W. G. Reinecke (ed.), Technomic Publishing, Lancaster, PA, pp. 962–969 (1999).

[15]Raftenberg, M. N., *Response of the Wayne State Thorax Model with Fabric Vest to a 9-mm Bullet*, ARL-TR-2897, Army Research Laboratory, Aberdeen Proving Ground, MD (Jan 2003).

ACKNOWLEDGMENTS: The authors would like to express their appreciation to the Office of Naval Research under contract number N00024-98-D-8124 for funding this work and to Gary Peck, Steve Main, Antonio Munoz, and Bob Wright for their contributions to this work.

THE AUTHORS

Jack C. Roberts, Principal Investigator (PI), leads APL's research in ballistic impact and blast effects on the human body. He is a member of the Principal Professional Staff in APL's Technical Services Department (TSD), with a joint appointment as a Research Professor in Mechanical Engineering at JHU. Dr. Roberts has 30 years of experience in structures, composite materials, and biomechanics and provides overall direction of the experimental and computational aspects of ballistic impact and blast effects. **Paul J. Biermann** is a member of the Senior Professional Staff in TSD with 25 years of experience in materials, process engineering, and prototype fabrication. He provides expertise in materials selection, modification, sensor integration, and molding processes. **James V. O'Connor** is Attending Surgeon and Director of Thoracic and Vascular Surgery at the R. Adams Crowley Shock Trauma Center. In addition to his M.D., Dr. O'Connor has a B.S. in electrical engineering and an M.S. in biomedical engineering. **Emily E. Ward** is a member of the Associate Professional Staff in TSD. She has worked on applications involving mechanical structural design and analysis, biomedical finite element modeling and analysis, and materials characterization. **Russell P. Cain** is a member of the Principal Professional Staff in TSD. With more than 20 of years experience in electrical systems, Mr. Cain provides expertise on sensors, data acquisition, sensor integration, and system control. **Bliss G. Carkhuff** is a member of the Senior Professional Staff in TSD and provides expertise in sensor signal conditioning and data collection and analysis. **Andrew C. Merkle** is a Biomedical Engineer in APL's National Security Technology Department and specializes in biomechanics and human injury prevention. Mr. Merkle was involved in the development of the surrogate torso, conducted ballistic and blast trials on the physical model, and worked to validate the computational model. Further information on APL research in ballistics and blast effects on the human body can be obtained from Dr. Jack Roberts. His e-mail address is jack.roberts@jhuapl.edu.


Jack C. Roberts


Paul J. Biermann

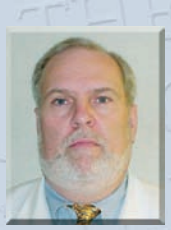
James V. O'Connor


Emily E. Ward


Russell P. Cain

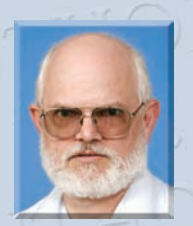
Bliss G. Carkhuff


Andrew C. Merkle